Provided for non-commercial research and education use.
Not for reproduction, distribution or commercial use.

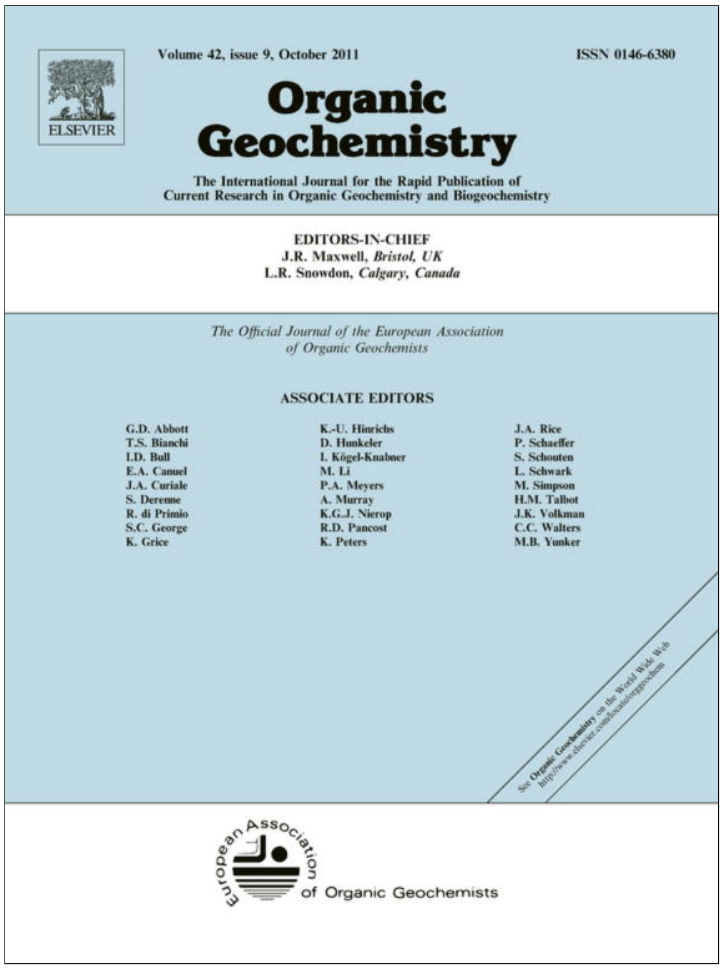

This article appeared in a journal published by Elsevier. The attached copy is furnished to the author for internal non-commercial research and education use, including for instruction at the authors institution and sharing with colleagues.

Other uses, including reproduction and distribution, or selling or licensing copies, or posting to personal, institutional or third party websites are prohibited.

In most cases authors are permitted to post their version of the article (e.g. in Word or Tex form) to their personal website or institutional repository. Authors requiring further information regarding Elsevier's archiving and manuscript policies are encouraged to visit:

http://www.elsevier.com/copyright

Author's personal copy

Organic Geochemistry 42 (2011) 1055–1064

Contents lists available at ScienceDirect

Organic Geochemistry

journal homepage: www.elsevier.com/locate/orggeochem

C 1s K-edge near edge X-ray absorption fine structure (NEXAFS) spectroscopy for characterizing functional group chemistry of black carbon

Karen Heymann [a], Johannes Lehmann [a,*], Dawit Solomon [a], Michael W.I. Schmidt [b], Thomas Regier [c]

[a] Department of Crop and Soil Sciences, Cornell University, Ithaca, NY, USA
[b] University of Zürich, Department of Geography, Winterthurerstrasse 190, CH-8056 Zürich, Switzerland
[c] Canadian Light Source Inc., Saskatoon, Saskatchewan, Canada S7N 5A8

ARTICLE INFO

Article history:
Received 8 September 2010
Received in revised form 17 June 2011
Accepted 29 June 2011
Available online 12 July 2011

ABSTRACT

Black carbon (BC) is considered ubiquitous in soil organic matter (OM) and therefore plays an important role in soil biogeochemistry. Its complexity, particularly within environmental matrices, presents a challenge for research, primarily as a result of techniques which may favor detection of certain functional group types rather than capturing total sample C. The objective of this study was to utilize carbon (C) 1s near edge X-ray absorption fine edge structure (NEXAFS) spectroscopy to characterize the C chemistry of a broad range of BC materials. Characteristic resonances in the NEXAFS spectra allowed direct molecular speciation of the total C chemistry of the reference materials, environmental matrices and potentially interfering materials, obtained from an earlier BC ring trial. Spectral deconvolution was used to further identify the functional group distribution of the materials. BC reference materials and soils were characterized by a large aromatic C region comprising around 40% of total absorption intensity. We were able to distinguish shale and melanoidin from BC reference materials on the basis of their unique spectral characteristics. However, bituminous coal shared chemical characteristics with BC reference materials, namely high aromaticity of more than 40% identified by way of a broad peak. Lignite also shared similar spectra and functional group distributions to BC reference materials and bituminous coal. We compared the results of spectral deconvolution with the functional group distributions obtained by way of direct polarization magic angle spinning (DPMAS) ^{13}C nuclear magnetic resonance (NMR) spectroscopy. Correlations between aromatic type C values for DPMAS ^{13}C NMR and NEXAFS gave $r^2 = 0.633$ ($p < 0.05$) and the values for NEXAFS were around 30–40% lower than for ^{13}C NMR. Correlations were also drawn between the aromatic C/O-alkyl C ratio values for the two methods ($r^2 = 0.49$, $p < 0.05$). Overall, NEXAFS was applicable for a wide range of environmental materials, such as those measured, although some limitations for the technique were addressed.

© 2011 Elsevier Ltd. All rights reserved.

1. Introduction

The black carbon (BC) continuum describes residues from the incomplete combustion of either biomass or fossil fuels (Schmidt and Noack, 2000; Preston and Schmidt, 2006). These combustion products reside largely in soil and sediments, and therefore play an important role in biogeochemical cycles (Czimczik and Masiello, 2007). BC serves as an important source and sink for global carbon (C) (Kuhlbusch, 1998; Masiello and Druffel, 1998) and is known to affect a multitude of soil properties and processes, such as cation exchange capacity (Liang et al., 2006), nutrient dynamics (Lehmann et al., 2003) and microbial habitation (Pietikäinen et al., 2000). The profound sorption of hydrophobic organic contaminants by BC in soil and marine sediments has long been observed (Cornelissen et al., 2004; Xiao et al., 2004). Despite increased attention to BC over the last decade, many questions remain regarding its chemistry and subsequent influence on reactivity, recalcitrance, residence time, transport and accumulation in terrestrial and aquatic systems.

The forms of BC most relevant to terrestrial and marine biogeochemistry may be divided into two broad categories: soot, which is formed at high temperatures from the condensation of hydrocarbons in the vapor phase (Akhter et al., 1985a; Preston and Schmidt, 2006) and char, formed directly from biomass at lower temperatures than soot (<700 °C) under oxygen deprived conditions (Fernandes and Brooks, 2003; Hopkins et al., 2007). Natural and anthropogenic addition of BC strongly affects the chemical signature of soil (Carter et al., 2002). For example, the accumulation of highly refractory aryl structures in Amazonian Dark Earths, attributed to the addition of biomass derived BC several hundred to a few thousand years ago, was suggested to be responsible for the biochemical recalcitrance and stability of soil organic C (Solomon et al., 2007). Surface chemistry can strongly influence the fate of

* Corresponding author. Tel.: +1 607 254 1236; fax: +1 607 255 3207.
E-mail address: CL273@cornell.edu (J. Lehmann).

0146-6380/$ - see front matter © 2011 Elsevier Ltd. All rights reserved.
doi:10.1016/j.orggeochem.2011.06.021

Author's personal copy

BC; for example, the extent of surface oxidation of atmospheric BC (soot, aerosols) can increase oxygen and defective structures at particles interfaces, promoting higher reactivity (Chughtai et al., 2002). Organic matter (OM) from Amazonian Dark Earths was observed to be enriched in aromatic C, O-rich C (carboxylic, aldehyde, ketone, quinone) and a diverse group of refractory alkyl C moieties. In contrast, OM from adjacent soil (unamended with BC) was predominantly composed of O-alkyl C and more labile alkyl C structures (Solomon et al., 2007). This trend of enrichment by BC is seen for a number of soils affected by fire regimes over long time spans (Skjemstad et al., 1999).

The complex surface and bulk chemistry of BC are not thoroughly understood due to highly variable formation conditions and until recently, a lack of international reference standards for cross comparison among different studies and laboratories (Schmidt et al., 2001). The combustion continuum encompasses the chemical and physical properties used to describe BC forms, ranging from partially charred plant biomass to highly ordered soot and graphite (Baldock et al., 2004). The chemical properties of BC are dependent on pyrolysis conditions and fuel type; for example, the charring of even simple components of biomass (lignin, cellulose, wood) affords structural changes that vary with the material, temperature and duration of charring (Reeves et al., 2007). The major defining characteristic is the presence of fused aromatic C ring structures, which become progressively ordered and condensed with increasing formation temperature (Schmidt and Noack, 2000). Carbon is a unique and versatile element as a result of the nearly infinite number of compounds it may form. This relates to the types of possible C bonds, the number of elements it can bond to and the different hybridization states of the bonds (sp^2, sp^3 or mixed hybridization states). Graphite, for example, is made up of a highly ordered periodic stack of graphene sheets comprising a hexagonal lattice with strong sp^2 bonding, i.e. 100% sp^2 hybridization. Amorphous C, by contrast, has a mixture of sp^2 and sp^3 bonds and displays no long range order. Using scanning electron microscopy (SEM), Brodowski et al. (2005) observed that soil BC occurred as both well-defined and amorphous particles. Lignocellulose biomass is transformed from relatively amorphous C structures to polyaromatic graphene sheets with increasing temperature, while low temperature BC is likely to be a complex mixture of these two main C forms (Nguyen et al., 2010). Thorough characterization of the BC continuum therefore necessitates detection of all C bonding states present in a sample.

In order to further our understanding of BC chemistry and its role in the environment, the utilization of advanced spectroscopic techniques is required. Many techniques (thermal, chemical, optical) employed for its characterization in soil and sediments are often optimized to detect only a portion of the chemical species present. This presents a challenge because of the broad range of characteristics comprising the combustion continuum. Studies have been employed to determine the part of the BC spectrum which is actually quantified with different methods (Elmquist et al., 2006). Solid state ^{13}C nuclear magnetic resonance (NMR) spectroscopy is widely used for the study of soil, natural OM, BC and marine sediments and is considered an accurate, semi-quantitative method for obtaining detailed information about the bulk chemistry of solid samples. Certain difficulties are, however, encountered in ^{13}C NMR studies of BC, which would benefit from the availability of additional spectroscopic techniques. Typical cross polarization (CP) ^{13}C NMR, may not detect 100% of BC carbon. This is due to the lack of protons in the highly aromatic structure, which are necessary to achieve detection (Hedges et al., 2000). Improved Bloch-decay (BD) or direct polarization (DP) techniques are available, but are not commonly used because of extensive sample run times (Hedges et al., 2000) or difficulties in obtaining good NMR spectra from biochar produced at high temperatures (Freitas et al., 1999; Bourke et al., 2007). The high electrical conductivity associated with the alignment of aromatic sheets may make measurement difficult and may result in peak shifting due to the presence of delocalized π-electrons in aromatic structures (Freitas et al., 2002).

NEXAFS spectroscopy is a powerful counterpart for the chemical characterization of BC or other complex environmental materials as it may overcome some of the aforementioned limitations of other techniques. It uses the intense, tunable, polarized X-ray beams generated by a synchrotron light source to probe the electronic states of a sample (Watts et al., 2006) and is able to capture total sample C. It probes the X-ray absorption cross section of a sample through inner-shell excitation processes; at photon energy close to an atomic absorption edge, inner shell electrons are excited to an unoccupied energy level, creating resonance peaks in the absorption spectra (Stöhr, 1992). Detection methods for these resonances include total electron yield (TEY), which can be used for probing sample surfaces (ca. 10 nm) and fluorescence yield (FLY), which is bulk sensitive and can be used to probe ca. 100 nm into the sample surface. FLY may be particularly useful for environmental samples such as soil, since electron yield from a sample depends on the charge transport properties of the sample.

NEXAFS is particularly suited for the characterization of complex heterogeneous samples such as BC, since absorption spectra depend directly on the local bonding environment of atoms (Lehmann and Solomon, 2010). When coupled with scanning transmission X-ray microscopy (STXM), NEXAFS is one of the few approaches to map the nano-scale heterogeneity of soil particles with sub-micron resolution (Kirz et al., 1995; Jacobsen et al., 2000; Lehmann and Solomon, 2010). Determining the functional group chemistry at high spatial resolution has proven vital in demonstrating biogeochemically relevant processes for BC in soil (Lehmann et al., 2005; Liang et al., 2006, 2008). However, little published information exists regarding the characterization of different BC forms using C NEXAFS. Keiluweit et al. (2010) used it to relate chemical changes occurring in char as a function of formation temperature and starting material to observed physical changes. Hopkins et al. (2007) observed that NEXAFS spectra from three samples of soot produced from diffusion flames (ethylene, methane, *n*-hexane) were very similar to each other, but distinct in functional composition from other types of soot, such as diesel soot. This demonstrates the powerful capabilities of NEXAFS in detecting fine-scale characteristics for distinguishing BC forms.

The main objectives of this research were to (i) characterize the C chemistry of contrasting forms of BC materials, (ii) determine the value of NEXAFS in distinguishing different BC types and non-BC OM in terrestrial ecosystems and (iii) assess the value of NEXAFS for obtaining spectra of environmentally complex samples such as BC. To date, no NEXAFS study is available that attempts to quantify the functional group chemistry of different BC types relevant for biogeochemical processes in soil and sediments.

2. Materials and methods

2.1. Materials

Reference materials identified by the BC steering committee (Schmidt et al., 2003; Hammes et al., 2007) were used. Descriptions of them can be found at http://www.geo.uzh.ch/phys/bc. They are categorized into three groups: (i) BC reference materials – *n*-hexane soot, grass char and wood char and (ii) environmental matrices – aerosol (urban dust NIST 1649a), marine sediment (NIST 1941b), a sand-rich Chernozem, a clay-rich Vertisol and dissolved OM from the Suwannee river and (iii) potentially interfering material –

Author's personal copy

melanoidin, shale, bituminous coal (Pocahontas) and lignite coal (Beulah-Zap).

2.2. Sample preparation

The reference materials were mixed with C-free nanopure water (0.5 mg/ml water) in 5 ml Eppendorf vials. The vials were lowered briefly into an ultrasound bath in order to achieve homogeneous wetting of the samples. Using a pipette, ca. 1 ml of sample solution was deposited onto Au coated Si wafers. The wafers were prepared by thermally evaporating an optically opaque layer of pure Au onto the unpolished side of commercially available Si wafers. The thermal evaporation used a 0.25 mm thick W filament wetted with Au (Lesker, 99.9%). Deposition was at 10^{-5} Torr and, once prepared, the substrates were left under vacuum until shortly before sample preparation and NEXAFS measurements.

2.3. Sample measurement

C (1s) NEXAFS spectra were obtained on beamline 11ID-1 at the Canadian Light Source (CLS) located at the University of Saskatchewan, Saskatoon, Canada. The beamline was equipped with a spherical grating monochromator (SGM) designed for high resolution soft X-ray spectroscopy (Regier et al., 2007). FLY was measured using a chevron stacked micro-channel pate (MCP) detector with a bias of −1600 V. The detector was at the same elevation as the sample, making an angle of 43° with respect to the beam axis. A negatively charged grid in front of the detector was used to repel electrons from the detector. The prepared sample plate was loaded into a vacuum chamber ($1e^{-7}$ Torr). The beamline was configured for a resolving power of ca. 7500 at the C K edge (exit slit gap 50 μm) and the photon energy was scanned from 270 to 310 eV. Dwell time was 0.5 s. Background measurements were taken by measuring an empty Au wafer on each sample plate loaded into the chamber. A normalization current was also measured during each scan by collecting the TEY from an Au mesh. The mesh was monitored for C contamination and was periodically refreshed using an in situ Au evaporator incorporated into the beamline vacuum system. A Ti filter was used in the beamline to reduce the effects of 2nd order oxygen in the pre-edge region. Two measurements were taken for each sample at different spots on the sample to make sure that the resulting spectra were identical. If inconsistency was observed, additional measurements were taken. Main 1s-π^* and Rydberg/mixed valence transitions in the fine structure regions of C K-edge spectra recorded from BC ring trial samples span an energy range of 284–310 eV. The fine structures in the C (1s) NEXAFS region above 290 eV transitions tend to be broad and overlap with each other (Cody et al., 1998; Schäfer et al., 2003); therefore, only the main 1s-π^* transitions were used for interpretation of the NEXAFS results.

Spectra were background subtracted as follows:

$$I_{sub} = I_{(FLY,TEY)} - gold_{(FLY,TEY)}/I_o$$

where I_{sub} corresponds to the subtracted signal, $I_{(FLY,TEY)}$ to sample current from either FLY or TEY, and Io to the current from a Au mesh monitor located upstream from the sample. In order to correct for C contamination in the beamline optics, a linear transformation was applied to normalize the pre-edge region of the sample with the pre-edge region of clean Au measured at the beginning of the experimental run. Details of the method can be found in the Supplementary online methods.

All data were normalized prior to curve fitting using ATHENA 0.8.052 software (Ravel and Newville, 2005). The photon energy was calibrated to the C 1s → π^* resonance in CO gas at 287.38 eV. Spectra were characterized according to the peak assignments in Table 1. The samples were not expected to have any long range order, since the C in the sample was randomly oriented. Therefore, there should be no polarization effects.

2.4. Deconvolution of spectra

Peak resonances with specific bonding environments were assigned on the basis of the spectral signatures of pure chemical standards representative of specific functional groups (Solomon et al., 2009). In order to compare the chemistry of the different samples in a semi-quantitative way, a least squares fitting scheme was applied to the normalized spectra in the range 280–310 eV. The scheme was based on eight Gaussians (labeled "G-1", etc.) following the procedure suggested by Scheinost et al. (2001), with additional bands to account for substituted aryl C (G3) and an additional carbonyl group (G8) (Liang et al., 2008). Specific positions for the Gaussian bands are described in Table 1. The Gaussian curve component positions were verified by examining the spectra of previously measured standards as representatives of specific functional groups. An arctangent function was used to model the ionization step and was fixed at 290 eV. The full width at half maximum of the bands was set at 0.4 ± 0.2 eV, while the amplitude was floated during the fit. Deconvolution was performed by resolving spectra into individual arctangent and Gaussian curve components (G) using the ATHENA software. Spectral regions represented by Gaussian curves were described as being generally attributed to the following functional groups: overall aromatic type C was represented by the sum of the [G1 + G2 + G3] peaks (Table 1); aromatic C with side chain substituent (such as phenolic C) by the G4 peak; alkyl C by the G5 peak; carboxylic C by the G6 peak, and O-alkyl C by the sum of the [G7 + G8] peaks (Lehmann et al., 2009). The application of a Gaussian fitting procedure for the extraction of semi-quantitative information was validated by the diversity of C species in these samples. It is known that the C K edge resonances of individual chemical species measured with resolving power of ca. 7500 should show non-Gaussian line shapes. This is due to asymmetric broadening caused by chemically distinct C sites, each in turn broadened by coupling of the electronic and nuclear degrees of freedom. However, when the spectra of many similar but distinct C molecules are added together, as in the case of a complex organic system like a soil, the result will resemble a (Gaussian) broadened peak. Absorption intensity and transition intensity values (proportion as a percentage value) reflect the relative concentration of functional groups, since absolute concentration based on peak intensity cannot be determined with NEXAFS. Deconvolution values used in the context of this study are meant to be a comparative tool and not as an absolute quantification of functional groups, particularly where comparisons are made with values obtained from other instrumental methods (such as ^{13}C NMR).

2.5. Statistical analysis

Linear regressions were calculated for the correlations between NEXAFS and ^{13}C NMR values for total aromatic C and the aromatic/O-alkyl C ratio. They were calculated using SigmaPlot software with a $p \leqslant 0.05$.

3. Results

TEY (Table 2; Fig. 1) and FLY (Table 3; Fig. 2) were measured simultaneously. We were successful in obtaining TEY data for all the samples; however, FLY spectra for samples very high in C (all BC reference materials and coal) suffered from distortion due to self-absorption phenomena and were unusable. As a result of these

Author's personal copy

Table 1
C 1s NEXAFS approximate transition energy ranges and assignments of primary absorption peaks (median values are indicated as average values for final fit position for all 12 standards).

C form	Bond	Transition	Peak energy (eV)	Deconvolution curve	Fit position	Median
Aromatic C Quinone-C	C═O	1 s-π*	283–284.5	G1	284.5	284.4 (−0.1)
Aromatic C	C═C	1 s-π*	284.9–285.5	G2	285.4	285.4
Aromatic C	C═O	1 s-π*	285.8–286.2	G3	286.1	286.1
Aromatic C with substituent	C═C—OH C═O R—(C═O)—R′	1 s-π*	286–287.4	G4	286.7	286.8 (+0.1)
Alkyl C	C—H	1 s-π*	287–287.6	G5	287.6	287.7
Carboxylic C	R—COOH COO C═O	1s-3p/σ*	288–288.7	G6	288.4	288.4
O-alkyl C	C—OH	1 s-π*	289.2–289.5	G7	289.2	289.2
O-alkyl C/carbonyl	COO^-	1 s-π*	289.5–290.2	G8	289.9	289.9

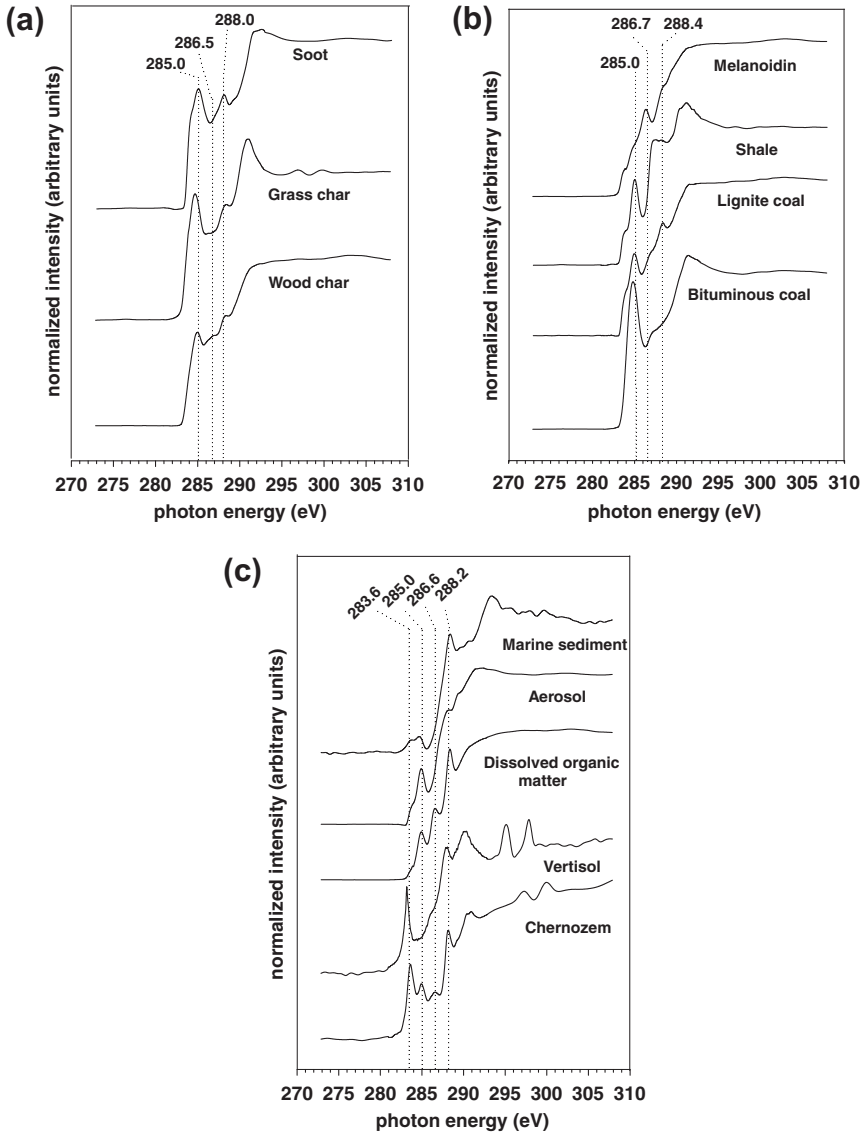

Fig. 1. C 1s NEXAFS total electron yield (TEY) spectra of: (a) BC reference materials, (b) potential interference products and (c) environmental matrices.

issues, only TEY results are discussed for all BC reference materials, as well as bituminous coal, lignite coal, melanoidin and shale, while both FLY and TEY results were discussed and compared for Vertisol, Chernozem, aerosol and dissolved OM. Comparison of both detection methods was included to illustrate a possible limitation of NEXAFS; the choice of detection method is critical when attempting to obtain quantitative data. A more detailed example of problems occurring during normalization as a result of self-

Author's personal copy

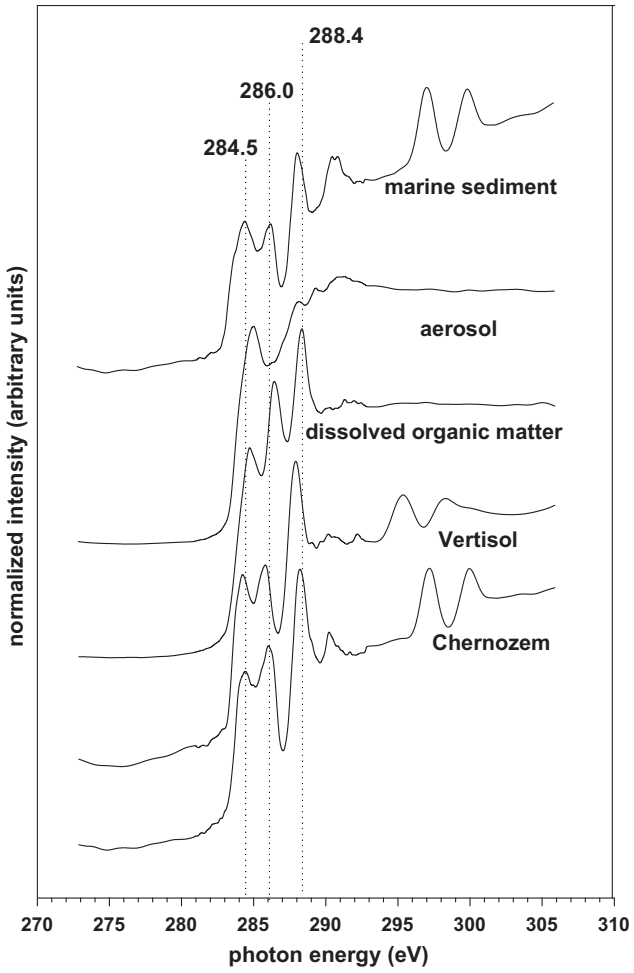

Fig. 2. C 1s NEXAFS fluorescence yield (FLY) spectra of environmental matrices.

absorption phenomena may be found in the Supplementary online material.

3.1. Characterization of BC reference materials

NEXAFS revealed a mixture of organic C bonding environments in the BC reference materials (Fig. 1a). The main characteristic was a broad, well resolved absorption band near 285 eV corresponding to the C 1s-$\pi^*_{C=C}$ transition, related to protonated and alkylated to carbonyl substituted aryl-C (C=C) (Cody et al., 1998; Coffey et al., 2002; Lehmann et al., 2005). The breadth can be attributed to multiple resonances, rather than an abundance of one type since additional absorption bands were observed as shoulders near 284.6 eV and 286.1 eV. The one at 284.6 eV, particularly apparent for soot, corresponds to the C 1s-π^* transition of quinone type C (C=O) structures such as benzoquinone, protonated and alkylated aromatic C and heteroatom-substituted aromatics (Jokic et al., 2003; Solomon et al., 2005). The broadness of the main aromatic transition suggested a complex chemical structure for the BC reference materials (di Stasio and Braun, 2006). Additional features beyond the aromatic region included multiple absorption bands as small shoulders near 286.5 eV and 288 eV, corresponding to the C 1s-π^*_{C-OH} and C 1s-$\pi^*_{C=O}$ transitions, representing mainly phenolic and carboxylic C, respectively. Wood char and grass char exhibited a carboxylic region shoulder centered at 288.4 eV, while the similar peak for soot was better resolved and centered at 288 eV. Solomon et al. (2009) identified a well-defined peak at 288.35 eV for benzoic acid, reflecting the C 1s-$\pi^*_{C=O}$ transition of carboxyl functional groups bonded to unsaturated C (Cody et al., 1998; Urquhart and Ade, 2002; Braun, 2005). The disparity in peak position between the soot and the chars near 288 eV may be attributed to soot having a more significant presence of two O atoms bonded to saturated C in carboxylic functional groups, rather than carboxylic groups bonded to unsaturated C, as in the case of wood and grass char (Solomon et al., 2009). An additional peak near 291 eV was observed for the soot and grass char; it has been assigned as representing the 1s-σ^* exciton in a study by Bernard et al. (2010) of high temperature chars.

Aromatic region values for the BC reference materials ranged from 39–47% (as a proportion of total absorption intensity), for grass char and wood char, to a value at the higher end for soot with 46%. Functional group distributions delineated by the individual Gaussian curves within the aromatic C region were similar among the BC reference materials (Table 2), ranging from 16–23% for G1, 15–21% for G2 and 3–7% for G3. The values indicate that BC reference materials contain high concentrations of quinone C and aryl type C, compared with O-substituted forms present at higher transitions such as phenolic type C. A significantly lower G5 value of 3% for grass char was observed vs. 18% for wood char and 19% for soot (Table 2). G6 region values were higher for grass char (20%) than wood char (14%) and soot (7%). O-alkyl regions were similar overall for wood char and grass char (23%), and soot (18%).

3.2. Characterization of environmental matrices

The aromatic regions of the Chernozem and Vertisol were characterized by two well resolved peaks near 284.5 and 286 eV (Fig. 1c). The aromatic C region was similar for Chernozem (46%) and Vertisol (40%) as detected with FLY (Table 3). Deconvolution values for the aromatic C region detected with TEY were also very similar between soils, with 41% for Chernozem and 39% for Vertisol in the aromatic C region. Despite the similar values for the two soil samples, functional group distributions were slightly different for the two detection methods, although both TEY and FLY attributed the majority of aromatic type C to the G1 regions. Deconvolution values for the G5–G7 regions were not in agreement between the two detection methods. This made it difficult to interpret the characteristic functional group contributions for the two soil types. Adding the values for the three regions together, we found that the resulting values were similar between the two detection methods. For the Vertisol and Chernozem, the [G5 + G6 + G7] values were 34% as detected with TEY; for the FLY data, the Chernozem value was 35% for this entire region, while the Vertisol value for the region was 38%. The complexity of the region, in addition to overlap of spectral bands, may therefore be an obstacle in obtaining more reliable values for environmental matrices. The sharp resonance (doublet) in the Vertisol spectra near 300 eV could be assigned to potassium $L_{2,3}$-edge absorption (Yoon et al., 2006).

Dissolved OM spectra revealed a highly heterogeneous structure, with three strongly resolved bands near 285, 286.5 and 288.4 eV corresponding to multiple C 1s-π^* transitions. The aromatic region comprised 22% (TEY) and 37% (FLY) of total absorption intensity, with the majority of transition intensity (13–20%) represented by the curve near 284.5 eV. The band near 286.7 eV represented nearly equivalent proportions of C detected with both TEY (17%) and FLY (14%). Similar proportions were calculated for the band near 287.6 eV, ca. 12% for both detection methods. The largest proportion of C for an individual band was calculated for the sharp transition near 288.4 eV, with 22% (TEY) and 18% (FLY), indicating a high concentration of acidic groups. The spectral signatures for dissolved OM were also in agreement for the two detection methods, although FLY peaks were better resolved and had improved intensity.

Aerosol was characterized by one main aromatic C transition at 284.9 eV and a small carboxylic shoulder at 288.3 eV, with

Author's personal copy

identical spectral patterns for both TEY and FLY. However, the FLY spectra revealed a signature highly comparable to the BC reference materials. Deconvolution gave contrasting results between the two methods since FLY attributed 22% of total absorption intensity to the G1 region vs. only 8% with TEY. Overall aromaticity in the aromatic C region was 19% (TEY) and 39% (FLY). Clearly, FLY detected twice the amount of aromatic C than TEY in the aromatic C region. Values for the G2–G6 region were similar (within 5% difference) for the two methods, but the G7 region and G8 region values were again very different (23% and 13% for TEY vs. 11% and 6% for FLY). In any case, the majority of absorption intensity appeared to fall within the G5–G8 region for aerosol (nearly 60% for TEY, 48% for FLY), indicating lower contribution from aromatic C compared with BC reference materials.

The marine sediment shared characteristics with the two soil samples; according to FLY, the aromatic region comprised 29% of total intensity. The marine sediment aromatic region accounted for only 6% according to TEY data. Like the soil, the marine sediment contained a low proportion of phenolic type C. The carboxylic C region made up a larger proportion (22%) and O-alkyl C made up 29% of total intensity. The spectral shapes for both methods were in agreement; however the TEY data attributed almost no C to the aromatic region, and the majority to the aliphatic (20%), carboxylic (31%) and O-alkyl (35%) regions.

3.3. Characterization of interference products

Bituminous coal, lignite coal and shale exhibited a pronounced band near ca. 285 eV, corresponding to the C 1s-$\pi^*_{C=C}$ transition related to aromatic C (Fig. 1b). Its appearance was broad and well resolved for bituminous coal and shale but relatively weak for lignite by visual comparison. Bituminous coal in particular was remarkably similar in spectral appearance to BC reference materials. The aromatic C region comprised a higher proportion of total absorption intensity for bituminous coal (46%) than lignite (34%) or shale (26%) (Tables 2 and 3). Lignite spectra revealed overlapping bands in the 286–289 eV region, while bituminous coal did not appear to show any notable characteristics in this region. A C 1s-$\pi^*_{C=C}$ transition at 287.8 eV for lignite appeared as a small peak. Shale spectra revealed a significant transition near 287 eV, possibly broadly overlapping regions between 287 and 290 eV, since no individual peaks were present in the region. Melanoidin was easily distinguished from other ring trial standards by way of the absence of a strong aromatic C 1s-$\pi^*_{C=C}$ transition, which was present only as a wide shoulder on a broad peak which had a maximum at 286.3 eV.

3.4. Correlations

We were able to utilize TEY data to make correlations between deconvolution data we obtained with NEXAFS and data collected with DPMAS ^{13}C NMR from a study by Hammes et al. (2008). Correlations between aromatic C (G1–G3) NEXAFS data and aryl C NMR data (Fig. 3) gave an r^2 value of 0.63 ($p < 0.05$). The aryl C/O-alkyl C ratio has been recommended as a parameter for comparing the decomposition of environmental samples (Baldock et al., 2004). We used it to further compare the results from DPMAS ^{13}C NMR and NEXAFS (Fig. 3). The [G1 + G2 + G3] region was summed to use as the aryl component, and the [G7 + G8] region was summed as the O-alkyl component. The r^2 value for the correlation was 0.49 ($p < 0.05$). The correlation values indicated that the ^{13}C NMR values were greater overall than the NEXAFS values. We also correlated the O-alkyl values for the two methods; however, the correlation was poor, and the r^2 value was ca. 0.1 ($p < 0.05$; data not shown).

4. Discussion

4.1. Identification of BC within environmental matrices

Aromaticity was the most distinct feature observed for BC, so was a possible signature for it in more complex matrices such as soil. The fingerprint in the aromatic C region for the two soil types was similar to the BC reference materials. The overall aromatic region was greater for the soil than for the other environmental matrices, and corresponded with the values for overall aromaticity of the BC reference materials, being nearly 40% of total absorption intensity according to deconvolution performed on TEY data. Upon closer inspection, the BC reference materials and the two soil samples exhibited similar distributions of transition intensity within the aromatic region (TEY data). However, FLY deconvolution values were not in agreement with TEY and showed all environmental matrices, including soil, to have similar proportions of absorption intensity within the aromatic region. FLY aromatic C values for environmental matrices could not be compared to those for BC, since FLY data for the BC materials were not obtainable, as discussed above.

The two soil samples exhibited individually unique spectral characteristics and functional group distributions, reflecting differences in labile OM as well as taxonomy and age. For example, the German Chernozem is a sandy soil that developed around 10,000 years ago. It is much younger than the Australian Vertisol, a clay soil. A previous study quantified the Chernozem as consisting of 50% BC as a fraction of total organic C (Schmidt et al., 1999)

Table 2
Deconvolution results for BC ring trial standards using C 1s NEXAFS total electron yield.[a]

	Proportion of absorption regions (%)						
	283–286.1	286–287.5	287.6–288.3	288.4–289.1	289.2–289.8	289.9–291.2	Chi^{2b}
Wood char	39	6	18	14	16	7	0.458
Grass char	41	12	3	20	9	14	0.019
Soot	47	10	19	7	13	5	0.170
Chernozem	41	7	6	21	13	12	0.176
Vertisol	39	13	16	5	19	9	0.342
Dissolved OM	22	17	12	22	12	14	0.023
Aerosol	19	8	16	21	23	13	0.077
Marine sediment	6	8	20	31	35	0	2.510
Bituminous coal	42	13	5	16	18	4	1.140
Lignite coal	34	11	10	20	24	1	0.055
Shale	26	8	25	10	21	9	0.596
Melanoidin	6	18	21	29	15	10	0.073

[a] Each value represents a proportion (%) of total absorption intensity within the region specified at the top of the column (refer to Table 1).
[b] Chi^2 value is statistical value provided for the model fit by ATHENA.

Author's personal copy

Table 3
Deconvolution results for BC ring trial standards using C 1s NEXAFS fluorescence yield.[a]

	Proportion of absorption regions (%)						
	283–286.1	286–287.5	287.6–288.3	288.4–289.1	289.2–289.8	289.9–291.2	Chi^2
Chernozem	46	6	15	14	11	8	0.846
Vertisol	40	7	8	23	13	8	0.680
Dissolved OM	37	14	13	18	6	14	0.489
Aerosol	39	7	17	20	11	6	0.094
Marine sediment	29	5	14	22	19	10	1.215
Shale	33	10	20	16	11	11	0.697
Melanoidin	34	21	23	1	14	6	0.032

[a] Each value represents a percentage of absorption intensity within the region specified at the top of the column (refer to Table 1).

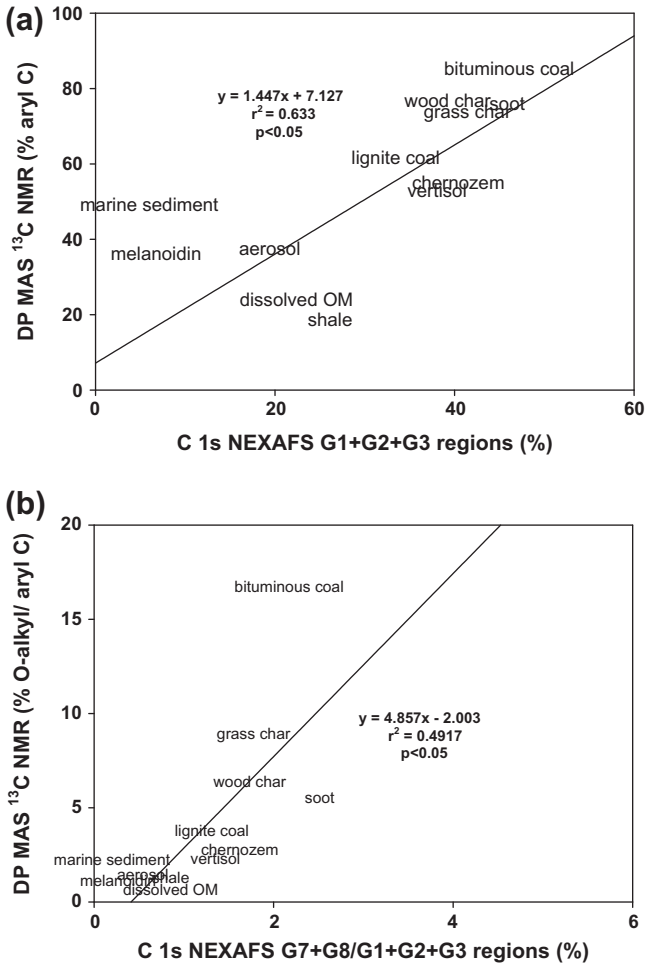

Fig. 3. (a) Correlation between concentrations of aryl C for ^{13}C NMR data from Hammes et al. (2008), and TEY data calculated for NEXAFS using spectral deconvolution; $p < 0.05$ and (b) correlation between aryl C/O-alkyl C values calculated for NEXAFS TEY data using spectral deconvolution and data from the study by Hammes et al. (2008); $p < 0.05$.

and the Vertisol with a comparatively lower BC concentration of 30% using photo-oxidation followed by ^{13}C NMR (Skjemstad et al., 1999). Schmidt et al. (1999) concluded that organic C in the German Chernozem was almost exclusively present as unsubstituted aromatic structures with negligible contributions from other species, using UV photo oxidation followed by ^{13}C NMR. In contrast, previous studies characterized the Vertisol as possessing abundant alkyl, O-alkyl, carbonyl and amide C components, attributable to the presence of polymethylene (lipid type) C, polysaccharides (cellulose), proteins and carboxylic acids (Skjemstad et al., 1999).

It was possible to make some observations relevant to BC signatures in the other environmental matrices. Aerosol has been characterized as containing some concentration of soot BC (fossil fuel derived) as well as a range of other materials, using chemical and thermal oxidation (Currie et al., 2002). The TEY results were consistent with these findings since the proportion of transition intensity in the aromatic region of aerosol was relatively lower than that of other environmental matrices, particularly when inspecting the values for the individual regions. Dissolved OM also indicated low values in the aromatic C region (TEY). BC has been identified in dissolved OM (Hockaday et al., 2006); however, a comparative study (Hammes et al., 2008) found that results for BC quantification in dissolved OM were variable, with different methods reporting both low (CTO-375) and higher estimates (TOT/R) for the same sample.

4.2. BC characterization

We observed spectral signatures among the BC reference materials that were similar to those observed for benzene carboxylic acids (Fig. S5) by Solomon et al. (2009), who utilized C 1s NEXAFS to compile a spectral library of standards relevant to the study of natural OM. The transitions for BC reference materials were therefore largely related to the C 1s-π^* transition characteristic of C—H sites of unsaturated C bonds (C=C) on aromatic ring structures (Cody et al., 1998). Both Baldock and Smernik (2002) and Fernandes and Brooks (2003) agreed that carbonaceous straw and wood char were dominated by highly aromatic (aryl dominated) structures. Di Stasio and Braun (2006) measured several soot types using C 1s NEXAFS spectroscopy and observed different spectral signatures depending on soot type, indicating that NEXAFS is capable of differentiating between BC reference materials. BC reference materials were also characterized by shoulders near 284.5 eV and 286 eV, which we attribute to additional aromatic ring structures similar to benzanthracene, at 284.3 eV by Solomon et al. (2009). These transitions represent C atoms with a double bond from benzene or diene structures, expected to be present in BC.

The complexity of the aromatic C region in BC has been explained as differences in bonding environment for highly aromatic C rings (di Stasio and Braun, 2006). The primary peak at 285 eV arises from the transition of the core (1s) electron to the valence π^* molecular orbital in aromatic C ring structures (Cody et al., 1995a), or from excitonic effects as observed by Bernard et al. (2010). Shifts in electronic transitions around the 285 eV aromatic peak that result from the attachment of other atoms such as O and H to these rings (e.g. quinone) are manifested as peak broadening in the aromatic C region. These energy shifts, which are the result of changes in polarization of the electron clouds around the C atoms, have been observed as a shoulder in ethylene soot and attributed (di Stasio and Braun, 2006) to the presence of benzoquinone (two C=O groups in an aromatic ring). However, the shoulder itself is a result of C atoms in the aromatic ring which are not

Author's personal copy

bound to O. The presence of benzoquinone-type C causes C atoms near O to experience a shift in absorption edge toward higher X-ray energy (oxidation), while the remainder experience a shift to lower energy (di Stasio and Braun, 2006). As a consequence of substitution in aromatic ring structures, peak broadening or even peak splitting may be observed in the aromatic region.

Soot and char spectra reflected the presence of some of O-containing moieties (carbonyl, carboxylic C) likely present on surfaces or edges, since most volatile matter was lost at the formation temperature. The presence of O in BC reference materials is an important aspect of their reactivity and long term stability in soil (Knicker et al., 2007). Fernandes and Brooks (2003) measured both wood and straw charcoal with ^{13}C CPMAS NMR, and observed 78–87% of total C as aromatic C, with small amounts of O-aromatic and O-alkyl C detected. Hammes et al. (2008) utilized ^{13}C NMR to characterize BC reference materials as comprising ca. 75% aryl C, and the remaining C as O-alkyl or carbonyl C. *n*-Hexane soot was shown to contain a variety of oxygen-containing functional groups, including alkyl ketones, aryl ethers, anhydrides and substituted aromatic groups (Akhter et al., 1985b). Within the C1s NEXAFS region it may be difficult to separate resonances attributed solely to C bonds from those related to C—O bonds within complex environmental materials as a result of extensive overlapping at the fine edge. In order to obtain finer detail concerning the molecular composition of BC standards, alternative techniques such as STXM may be required (Yoon et al., 2006).

4.3. Distinguishing BC forms in the environment

Our results indicate that the ability to differentiate between BC and some materials of non-pyrogenic origin may be confounded by observance of C signatures alone, whether by NEXAFS or alternative spectroscopic methods such as ^{13}C NMR. Our observations are in agreement with those of Hammes et al. (2008), who observed that the high degree of similarity between BC and coal presented difficulties for BC quantification with ^{13}C NMR, and that the H/C and O/C ratios and spectral features of bituminous coal were very similar to BC (char and soot). While NEXAFS offers an advantage over ^{13}C NMR in its high sensitivity and ability to detect all C bonding environments, the complexity of the resulting spectra may limit the "quantitativeness" of data analysis unless more sophisticated analyses are developed for complex environmental samples such as soil.

We observed that the bituminous coal signature was nearly identical to that of BC reference materials, and lignite was slightly lower in aromaticity than bituminous coal and exhibited a small additional peak at 288 eV. Therefore, the coals could not be distinguished clearly from BC reference materials according to the deconvolution results. For high volatility bituminous coal, the concentration of phenol is anticipated to be low, while in low rank coal a substantial proportion of the aromatic C is bonded to O, implying a complex near-edge structure (Cody et al., 1995b). No differences were detected in the phenolic C region; however, the disparity in the functional group distributions between the two coals was in the O-alkyl region, with lignite coal reflecting all band area in the G7 region, while the opposite trend was observed for bituminous coal, with most falling in the G8 region. The sharp peak that lignite coal exhibited in the carboxylic region may explain the higher band area in the G7 region, possibly because of some overlap. Cody et al. (1995b) identified the higher transition of an electron from the core (1s) to a mixed Rydberg valence (C—H*) state in bituminous coal; the intensity of this band correlated with alkyl C. However, deconvolution results in this study showed a relatively small proportion of total absorption intensity attributable to the alkyl C region in either coal, and much higher proportions were observed for carboxylic type C. Cody et al. (1995b) also observed that the intensity of the 288 eV shoulder was greatest for cutinite and lowest for inertinite, a trend consistent with expected variation in chemical structure and composition of macerals in bituminous coal, implying that the absorption at 288 eV is derived principally from the mixed Rydberg/C—H transition of aliphatic C. It is possible that the overlap of these two features confounded the deconvolution results, and that some proportion of what is observed as carboxylic C in our study is likely a reflection of alkyl C. Overall, we did not observe any clear distinctions between the deconvolution results from bituminous or lignite coal and the BC reference materials; however, we observed unique characteristics for the shale and melanoidin that clearly distinguished them from the BC reference materials. The melanoidin spectral fingerprint lacked the central aromatic C peak near 285 eV, which was the main feature of all the BC reference materials. Rather, the most intense peak appeared at 286.3 eV, in agreement with published NEXAFS spectra of melanoidin from Haberstroh et al. (2006), and was attributed to the presence of phenols. For the shale, NEXAFS spectral deconvolution attributed over half of total absorption intensity to alkyl or O-alkyl type C, comparable to the proportion Hammes et al. (2008) were able to distinguish from HF treated kerogen (shale) from BC reference materials on the basis of the alkyl C signal, which contributed 70% of total detected C, with very little aryl C detected. The shale used in this study has also been previously characterized as being low in aromaticity and high in alkyl biopolymers that constitute the cell walls of algae (Trewhella et al., 1986).

4.4. Methodological considerations

We relied heavily on TEY measurements for the interpretation of environmental matrices. BC measurements with FLY suffered from self-absorption, which caused distortion in the spectra and impacted negatively on data quality. This was a result of the material characteristics; self-absorption phenomena occur when highly concentrated particles are measured and results from particle size, which in this case was already quite small. We felt that it was important to present both detection methods, since improvements to the FLY method in particular should be explored in future studies. Additionally, interpretation of absorption values should be understood to reflect relative concentrations of functional groups. Absolute concentration based on peak intensity cannot be determined with NEXAFS, since absorption intensity is a function of the magnitude of the oscillator strength of the transition (Cody et al., 1995a). Deconvolution values used in the context of this study are meant to be a comparative tool for BC reference standards, and not an absolute quantification of functional groups, particularly where comparisons with values obtained from other instrumental methods (such as ^{13}C NMR) are made.

NEXAFS deconvolution values in the aromatic C regions were around 30–40% lower overall than in the comparable characterization study of these identical materials using CPMAS and DPMAS ^{13}C NMR by Hammes et al. (2008). The complexity of the C 1s NEXAFS spectra made it difficult to correctly identify poorly resolved species in complex samples. For example, we may have misinterpreted band structures in poorly resolved regions by assigning either too many or too few bands in a particular region. The complexity of environmental samples makes the assignment of a set deconvolution scheme for a wide range of samples challenging. In addition, fitting problems may have occurred because of poorly resolved overlapping bands. The limitations of DPMAS ^{13}C have been acknowledged, but are unlikely to be responsible for the problems observed with the fits to the NEXAFS data, particularly with regard to the aliphatic, carboxylic and O-alkyl C peak assignments, and our attempts to quantify them. Innovative fitting approaches are needed to improve the quantification of C groups in environmental samples.

Author's personal copy

5. Conclusions

We successfully characterized a broad range of materials from a BC ring trial including BC reference materials, potentially interfering materials and environmental matrices using C 1s NEXAFS. We were able to identify total aromaticity of around 40% as a common feature for both environmental matrices and the BC reference materials. However, we encountered certain limitations, despite the sophisticated data capturing capabilities offered by NEXAFS. Establishing distinct differences between plant biomass derived BC (wood char and grass char) and fossil fuel derived BC (soot) was not possible from the results obtained, due to the similarities between the spectral and deconvolution data for the samples. Advantages such as the ability to directly measure soil C in situ were mitigated by the disparity between deconvolution data from the two different detection methods, which were expected to yield similar results but did not in our more detailed analysis of specific spectral regions.

While NEXAFS spectroscopy has the advantage of obtaining high resolution spectra for a wide range of environmental materials, including those encompassed in the BC combustion continuum, the "quantitativeness" of deconvolution methods will be limited until improved experimental techniques can be developed. It is also important to note that issues with FLY data may arise if the sample of interest is concentrated in particles (such as BC), regardless of concentration, which may limit the resolution attainable for BC using NEXAFS. In the future, more extensive research into deconvolution techniques for environmental samples with known chemistry is warranted in order to maximize the potential of this advanced spectroscopic method.

Acknowledgments

The authors acknowledge the helpful support of R. Blyth. We also thank K. Hanley for help in the laboratory. S. di Stasio and A. Braun are thanked for the spectra. We are grateful for the constructive comments by two anonymous reviewers. The study was supported by grants from the NSF IGERT Program (BCS-0215890), the NSF-Geobiology (EAR-0819689), USDA-AFRI (2008-35107-04511) and the Department of Crop and Soil Sciences at Cornell University. Any opinions, findings and conclusions or recommendations expressed are those of the authors and do not necessarily reflect the views of the National Science Foundation.

Appendix A. Supplementary material

Supplementary data associated with this article can be found, in the online version, at doi:10.1016/j.orggeochem.2011.06.021.

Associate Editor—**S. Derenne**

References

Akhter, M.S., Chughtai, A.R., Smith, D.M., 1985a. Aromaticity of elemental carbon (soot) by ^{13}C CP/MAS and FT-IR spectroscopy. Carbon 23, 593–594.

Akhter, M.S., Chughtai, A.R., Smith, D.M., 1985b. The structure of hexane soot-I. Spectroscopic studies. Applied Spectroscopy 39, 143–153.

Baldock, J.A., Masiello, C.A., Gelinas, Y., Hedges, J.I., 2004. Cycling and composition of organic matter in terrestrial and marine ecosystems. Marine Chemistry 92, 39–64.

Baldock, J.A., Smernik, R.J., 2002. Chemical composition and bioavailability of thermally altered Pinus resinosa (Red pine) wood. Organic Geochemistry 33, 1093–1109.

Bernard, S., Beyssac, O., Benzerara, K., Findling, N., Tzvetkov, G., Brown Jr., G.E., 2010. Raman and XRD study of anthracene-based cokes and saccharose-based chars submitted to high temperature pyrolysis. Carbon 48, 2506–2516.

Bourke, J., Manley-Harris, M., Fushimi, C., Dowaki, K., Nunoura, T., Antal, M.J., 2007. Do all carbonized charcoals have the same chemical structure? 2. A model of the chemical structure of carbonized charcoal. Industrial and Engineering Chemistry Research 46, 5954–5967.

Braun, A., 2005. Carbon speciation in airborne particulate matter with C (1s) NEXAFS spectroscopy. Journal of Environmental Monitoring 7, 1059–1065.

Brodowski, S., Amelung, W., Haumaier, L., Abetz, C., Zech, W., 2005. Morphological and chemical properties of black carbon in physical soil fractions as revealed by scanning electron microscopy and energy-dispersive X-ray spectroscopy. Geoderma 128, 116–129.

Carter, M.R., Skjemstad, J.O., MacEwan, R.J., 2002. Comparison of structural stability, carbon fractions and chemistry of krasnozem soils from adjacent forest and pasture areas in south-western Victoria. Australian Journal of Soil Research 40, 283–298.

Chughtai, A.R., Kim, J.M., Smith, D.M., 2002. The effect of air/fuel ratio on properties and reactivity of combustion soots. Journal of Atmospheric Chemistry 43, 21–43.

Cody, G.D., Botto, R.E., Ade, H., Behal, S., Disko, M., Wirick, S., 1995a. Inner-shell spectroscopy and imaging of a sub-bituminous coal – in-situ analysis of organic and inorganic microstructure using C(1s)-NEXAFS, Ca(2p)-NEXAFS, and C1(2s)-NEXAFS. Energy & Fuels 9, 525–533.

Cody, G.D., Botto, R.E., Ade, H., Behal, S., Disko, M., Wirick, S., 1995b. C-NEXAFS microanalysis and scanning-X-ray microscopy of microheterogeneities in a high-volatile bituminous coal. Energy & Fuels 9, 75–83.

Cody, G.D., Ade, H., Wirick, S., Mitchell, G.D., Davis, A., 1998. Determination of chemical-structural changes in vitrinite accompanying luminescence alteration using C-NEXAFS analysis. Organic Geochemistry 28, 441–455.

Coffey, T., Urquhart, S.G., Ade, H., 2002. Characterization of the effects of soft X-ray irradiation on polymers. Journal of Electron Spectroscopy and Related Phenomena 122, 65–78.

Cornelissen, G., Elmquist, M., Groth, I., Gustafsson, O., 2004. Effect of sorbate planarity on environmental black carbon sorption. Environmental Science and Technology 38, 3574–3580.

Currie, L.A., Benner, B.A., Kessler, J.D., Klinedinst, D.B., Klouda, G.A., Marolf, J.V., Slater, J.F., Wise, S.A., Cachier, H., Cary, R., Chow, J.C., Watson, J., Druffel, E.R.M., Masiello, C.A., Eglinton, T.I., Pearson, A., Reddy, C.M., Gustafsson, O., Quinn, J.G., Hartmann, P.C., Hedges, J.I., Prentice, K.M., Kirchstetter, T.W., Novakov, T., Puxbaum, H., Schmid, H., 2002. A critical evaluation of interlaboratory data on total, elemental, and isotopic carbon in the carbonaceous particle reference material, NIST SRM 1649a. Journal of Research of the National Institute of Standards and Technology 107, 279–298.

Czimczik, C.I., Masiello, C.A., 2007. Controls on black carbon storage in soils. Global Biogeochemical Cycles 21, 1–8.

di Stasio, S., Braun, A., 2006. Comparative NEXAFS study on soot obtained from an ethylene/air flame, a diesel engine, and graphite. Energy & Fuels 20, 187–194.

Elmquist, M., Cornelissen, G., Kukulska, Z., Gustafsson, O., 2006. Distinct oxidative stabilities of char versus soot black carbon: implications for quantification and environmental recalcitrance. Global Biogeochemical Cycles 20, 1–11.

Fernandes, M.B., Brooks, P., 2003. Characterization of carbonaceous combustion residues: II. Nonpolar organic compounds. Chemosphere 53, 447–458.

Freitas, J.C.C., Bonagamba, T.J., Emmerich, F.G., 1999. ^{13}C high-resolution solid-state NMR study of peat carbonization. Energy & Fuels 13, 53–59.

Freitas, J.C.C., Passamani, E.C., Orlando, M.T.D., Emmerich, F.G., Garcia, F., Sampaio, L.C., Bonagamba, T.J., 2002. Effects of ferromagnetic inclusions on ^{13}C MAS NMR spectra of heat-treated peat samples. Energy & Fuels 16, 1068–1075.

Haberstroh, P.R., Brandes, J.A., Gelinas, Y., Dickens, A.F., Wirick, S., Cody, G., 2006. Chemical composition of the graphitic black carbon fraction in riverine and marine sediments at sub-micron scales using carbon X-ray spectromicroscopy. Geochimica et Cosmochimica Acta 70, 1483–1494.

Hammes, K., Schmidt, M.W.I., Smernik, R.J., Currie, L.A., Ball, W.P., Nguyen, T.H., Louchouarn, P., Houel, S., Gustafsson, O., Elmquist, M., Cornelissen, G., Skjemstad, J.O., Masiello, C.A., Song, J., Peng, P., Mitra, S., Dunn, J.C., Hatcher, P.G., Hockaday, W.C., Smith, D.M., Hartkopf-Froeder, C., Boehmer, A., Luer, B., Huebert, B.J., Amelung, W., Brodowski, S., Huang, L., Zhang, W., Gschwend, P.M., Flores-Cervantes, D.X., Largeau, C., Rouzaud, J.N., Rumpel, C., Guggenberger, G., Kaiser, K., Rodionov, A., Gonzalez-Vila, F.J., Gonzalez-Perez, J.A., de la Rosa, J.M., Manning, D.A.C., Lopez-Capel, E., Ding, L., 2007. Comparison of quantification methods to measure fire-derived (black/elemental) carbon in soils and sediments using reference materials from soil, water, sediment and the atmosphere. Global Biogeochemical Cycles 21, 1–18.

Hammes, K., Smernik, R.J., Skjemstad, J.O., Schmidt, M.W.I., 2008. Characterisation and evaluation of reference materials for black carbon analysis using elemental composition, colour, BET surface area and ^{13}C NMR spectroscopy. Applied Geochemistry 23, 2113–2122.

Hedges, J.I., Eglinton, G., Hatcher, P.G., Kirchman, D.L., Arnosti, C., Derenne, S., Evershed, R.P., Kögel-Knabner, I., de Leeuw, J.W., Littke, R., Michaelis, W., Rullkotter, J., 2000. The molecularly-uncharacterized component of nonliving organic matter in natural environments. Organic Geochemistry 31, 945–958.

Hockaday, W.C., Grannas, A.M., Kim, S., Hatcher, P.G., 2006. Direct molecular evidence for the degradation and mobility of black carbon in soils from ultrahigh-resolution mass spectral analysis of dissolved organic matter from a fire-impacted forest soil. Organic Geochemistry 37, 501–510.

Hopkins, R.J., Lewis, K., Desyaterik, Y., Wang, Z., Tivanski, A.V., Arnott, W.P., Laskin, A., Gilles, M.K., 2007. Correlations between optical, chemical and physical properties of biomass burn aerosols. Geophysical Research Letters 34, 573–591.

Jacobsen, C., Wirick, S., Flynn, G., Zimba, C., 2000. Soft X-ray spectroscopy from image sequences with sub-100 nm spatial resolution. Journal of Microscopy – Oxford 197, 173–184.

Author's personal copy

Jokic, A., Cutler, J.N., Ponomarenko, E., van der Kamp, G., Anderson, D.W., 2003. Organic carbon and sulphur compounds in wetland soils: insights on structure and transformation processes using K-edge XANES and NMR spectroscopy. Geochimica et Cosmochimica Acta 67, 2585–2597.

Keiluweit, M., Nico, P.S., Johnson, M.G., Kleber, M., 2010. Dynamic molecular structure of plant biomass-derived black carbon (biochar). Environmental Science and Technology 44, 1247–1253.

Kirz, J., Jacobsen, C., Howells, M., 1995. Soft X-ray microscopies and their biological applications. Quarterly Reviews of Biophysics 28, 33–130.

Knicker, H., Muffler, P., Hilscher, A., 2007. How useful is chemical oxidation with dichromate for the determination of "Black Carbon" in fire-affected soils? Geoderma 142, 178–196.

Kuhlbusch, T.A.J., 1998. Black carbon and the carbon cycle. Science 280, 1903–1904.

Lehmann, J., Solomon, D., 2010. Organic carbon chemistry in soils observed by synchrotron-based spectroscopy. In: Singh, B., Gräfe, M. (Eds.), Synchrotron-based Techniques in Soils and Sediments. Elsevier, Amsterdam, pp. 289–312.

Lehmann, J., da Silva, J.P., Steiner, C., Nehls, T., Zech, W., Glaser, B., 2003. Nutrient availability and leaching in an archaeological Anthrosol and a Ferralsol of the Central Amazon basin: fertilizer, manure and charcoal amendments. Plant and Soil 249, 343–357.

Lehmann, J., Liang, B.Q., Solomon, D., Lerotic, M., Luizao, F., Kinyangi, J., Schäfer, T., Wirick, S., Jacobsen, C., 2005. Near-edge X-ray absorption fine structure (NEXAFS) spectroscopy for mapping nano-scale distribution of organic carbon forms in soil: application to black carbon particles. Global Biogeochemical Cycles 19, 1–12.

Lehmann, J., Brandes, J., Fleckenstein, H., Jacobsen, C., Solomon, D., Thieme, J., 2009. Synchrotron-based near-edge X-ray spectroscopy of natural organic matter in soils and sediments. In: Senesi, N., Xing, P., Huang, P.M. (Eds.), Biophysico-Chemical Processes Involving Natural Nonliving Organic Matter in Environmental Systems. IUPAC Series on Biophysico-Chemical Processes in Environmental Systems. Wiley, NJ, pp. 729–781.

Liang, B., Lehmann, J., Solomon, D., Kinyangi, J., Grossman, J., O'Neill, B., Skjemstad, J.O., Thies, J., Luizao, F.J., Petersen, J., Neves, E.G., 2006. Black carbon increases cation exchange capacity in soils. Soil Science Society of America Journal 70, 1719–1730.

Liang, B., Lehmann, J., Solomon, D., Sohi, S., Thies, J.E., Skjemstad, J.O., Luizao, F.J., Engelhard, M.H., Neves, E.G., Wirick, S., 2008. Stability of biomass-derived black carbon in soils. Geochimica et Cosmochimica Acta 72, 6069–6078.

Masiello, C.A., Druffel, E.R.M., 1998. Black carbon in deep-sea sediments. Science 280, 1911–1913.

Nguyen, B., Lehmann, J., Hockaday, W.C., Joseph, S., Masiello, C., 2010. Temperature sensitivity of black carbon decomposition and oxidation. Environmental Science and Technology 44, 3324–3331.

Pietikäinen, J., Kiikkila, O., Fritze, H., 2000. Charcoal as a habitat for microbes and its effect on the microbial community of the underlying humus. Oikos 89, 231–242.

Preston, C.M., Schmidt, M.W.I., 2006. Black (pyrogenic) carbon: a synthesis of current knowledge and uncertainties with special consideration of boreal regions. Biogeosciences 3, 397–420.

Ravel, B., Newville, M., 2005. Athena, artemis, hephaestus. Journal of Synchrotron Radiation 12, 537–541.

Reeves, J.B., McCarty, G.W., Rutherford, D.W., Wershaw, R.L., 2007. Near infrared spectroscopic examination of charred pine wood, bark, cellulose and lignin: implications for the quantitative determination of charcoal in soils. Journal of Near Infrared Spectroscopy 15, 307–315.

Regier, T., Krochak, J., Sham, T.K., Hu, Y.F., Thompson, J., Blyth, R.I.R., 2007. Performance and capabilities of the Canadian Dragon: the SGM beamline at the Canadian Light Source. Nuclear Instruments & Methods in Physics Research Section A – Accelerators Spectrometers Detectors and Associated Equipment 582, 93–95.

Schäfer, T., Hertkorn, N., Artinger, R., Claret, F., Bauer, A., 2003. Functional group analysis of natural organic colloids and clay association kinetics using C(1s) spectromicroscopy. Journal de Physique IV 104, 409–412.

Scheinost, A.C., Kretzschmar, R., Christl, I., Jacobsen, C., 2001. Carbon group chemistry of humic and fulvic acid: a comparison of C 1s NEXAFS and ^{13}C NMR spectroscopies. In: Ghabbour, E.A., Davies, G. (Eds.), Humic Substances: Structures, Models and Functions. Royal Society of Chemistry, Cambridge, UK, pp. 39–47.

Schmidt, M.W.I., Noack, A.G., 2000. Black carbon in soils and sediments: analysis, distribution, implications, and current challenges. Global Biogeochemical Cycles 14, 777–793.

Schmidt, M.W.I., Skjemstad, J.O., Gehrt, E., Kögel-Knabner, I., 1999. Charred organic carbon in German chernozemic soils. European Journal of Soil Science 50, 351–365.

Schmidt, M.W.I., Skjemstad, J.O., Czimczik, C.I., Glaser, B., Prentice, K.M., Gelinas, Y., Kuhlbusch, T.A.J., 2001. Comparative analysis of black carbon in soils. Global Biogeochemical Cycles 15, 163–167.

Schmidt, M.W.I., Masiello, C.A., Skjemstad, J.O., 2003. Final recommendations for reference materials in black carbon analysis. EOS 84, 582–583.

Skjemstad, J.O., Taylor, J.A., Smernik, R.J., 1999. Estimation of charcoal (char) in soils. Communications in Soil Science and Plant Analysis 30, 2283–2298.

Solomon, D., Lehmann, J., Kinyangi, J., Liang, B.Q., Schäfer, T., 2005. Carbon K-edge NEXAFS and FTIR-ATR spectroscopic investigation of organic carbon speciation in soils. Soil Science Society of America Journal 69, 107–119.

Solomon, D., Lehmann, J., Thies, J., Schäfer, T., Liang, B.Q., Kinyangi, J., Neves, E., Petersen, J., Luizão, F., Skjemstad, J., 2007. Molecular signature and sources of biochemical recalcitrance of organic C in Amazonian Dark Earths. Geochimica et Cosmochimica Acta 71, 2285–2298.

Solomon, D., Lehmann, J., Kinyangi, J., Liang, B.Q., Heymann, K., Dathe, L., Hanley, K., Wirick, S., Jacobsen, C., 2009. Carbon (1s) NEXAFS spectroscopy of biogeochemically relevant reference organic compounds. Soil Science Society of America Journal 73, 1817–1830.

Stöhr, J., 1992. NEXAFS Spectroscopy. Springer Series in Surface Sciences, vol. 25. Springer, Berlin, Germany.

Trewhella, M.J., Poplett, I.J.F., Grint, A., 1986. Structure of Green River oil-shale kerogen- determination using solid-state ^{13}C NMR-spectroscopy. Fuel 65, 541–546.

Urquhart, S.G., Ade, H., 2002. Trends in the carbonyl core (C 1s, O 1s) $\rightarrow \pi_{C=O}$ transition in the near-edge X-ray absorption fine structure spectra of organic molecules. Journal of Physical Chemistry B 106, 8531–8538.

Watts, B., Thomsen, L., Dastoor, P.C., 2006. Methods in carbon K-edge NEXAFS: experiment and analysis. Journal of Electron Spectroscopy and Related Phenomena 151, 105–120.

Xiao, B.H., Yu, Z.Q., Huang, W.L., Song, J.Z., Peng, P.A., 2004. Black carbon and kerogen in soils and sediments. 2. Their roles in equilibrium sorption of less-polar organic pollutants. Environmental Science and Technology 38, 5842–5852.

Yoon, T.H., Benzerara, K., Ahn, S., Luthy, R.G., Tyliszczak, T., Brown, G.E., 2006. Nanometer-scale chemical heterogeneities of black carbon materials and their impacts on PCB sorption properties: soft X-ray spectromicroscopy study. Environmental Science and Technology 40, 5923–5929.